AIP | The Journal of Chemical Physics

Energetic modeling and single-molecule verification of dynamic regulation on receptor complexes by actin corrals and lipid raft domains

Chien Y. Lin, Jung Y. Huang, and Leu-Wei Lo

Citation: The Journal of Chemical Physics **141**, 215102 (2014); doi: 10.1063/1.4902985
View online: http://dx.doi.org/10.1063/1.4902985
View Table of Contents: http://scitation.aip.org/content/aip/journal/jcp/141/21?ver=pdfcov
Published by the AIP Publishing

Energetic modeling and single-molecule verification of dynamic regulation on receptor complexes by actin corrals and lipid raft domains

Chien Y. Lin,[1] Jung Y. Huang,[2,a)] and Leu-Wei Lo[3]
[1]*Department of Photonics, Chiao Tung University, Hsinchu 300, Taiwan*
[2]*The T.K.B. Research Center of Photonics, Chiao Tung University, Hsinchu 300, Taiwan*
[3]*Institute of Biomedical Engineering and Nanomedicine, National Health Research Institutes, Zhunan, Miaoli 350, Taiwan*

(Received 9 September 2014; accepted 18 November 2014; published online 5 December 2014)

We developed an energetic model by integrating the generalized Langevin equation with the Cahn-Hilliard equation to simulate the diffusive behaviors of receptor proteins in the plasma membrane of a living cell. Simulation results are presented to elaborate the confinement effects from actin corrals and protein-induced lipid domains. Single-molecule tracking data of epidermal growth factor receptors (EGFR) acquired on live HeLa cells agree with the simulation results and the mechanism that controls the diffusion of single-molecule receptors is clarified. We discovered that after ligand binding, EGFR molecules move into lipid nanodomains. The transition rates between different diffusion states of liganded EGFR molecules are regulated by the lipid domains. Our method successfully captures dynamic interactions of receptors at the single-molecule level and provides insight into the functional architecture of both the diffusing EGFR molecules and their local cellular environment.
 [http://dx.doi.org/10.1063/1.4902985]

I. INTRODUCTION

Live cells must execute a variety of cellular processes to survive in a changing environment.[1–5] The signaling process is responsible for relaying messages from the external environment to the cell nucleus. The first event of cellular signaling occurs at various types of receptors in the plasma membrane of a live cell. To faithfully estimate a signal that varies in space and time, a living cell faces the optimization problem of placing a collection of distributed and mobile receptors by balancing two opposing objectives. The first objective is the need to locally assemble sensors to reduce estimation noise and the second is the need to spread them to reduce spatial error. Recently Iyengara and Rao provided a fresh perspective on the optimization problem based on information theory.[6] They arrived two optimal strategies in the context of biology: The signaling protein receptors on the surface of live cells can be organized into a stationary lattice architecture or into a mobile active clustering depending on the local density of receptors and the incoming signal characteristics.

However, the real situation is much more complex because living eukaryotic cells are highly heterogeneous and stochastically dynamic. Lipid nanodomains (lipid rafts), which are rich in saturated lipid and cholesterol,[7,8] can be formed spontaneously. It had been known that lipid raft domains also contain several kinds of actin-anchored receptor proteins.[7] Phosphoinositides, which are the widely noted actin regulator, can directly interact with those actin-anchored proteins and induce an aggregation of actin filaments underneath the lipid raft domains.[9–11] The local density increases of actin filaments can serve as the nucleation sites for the formation of stable lipid domains. Thus, a correlation between the formation dynamics of lipid rafts and the remodeling of actin network may exist. The correlated dynamics could be imposed on the diffusive behaviors of actin-anchored membrane proteins.[12–14] Kusumi *et al.* proposed a cooperative action model that involves a hierarchical structure of actin skeleton-induced membrane compartments, lipid raft domains, and dynamic protein complexes.[15] However to verify the underlying processes are energetically favorable, it is important to develop an energetic model based on fundamental laws. The model may also be useful to help retrieving important information from single-molecule trajectories.

In this study, we integrated the generalized Langevin equation[16] with the Cahn–Hilliard equation[17,18] into a unified formalism. The resulting energetic model involves a hierarchical structure of actin corrals, protein-induced lipid ordering domains, and dynamic receptor proteins. Simulation results are presented to elaborate the confinement effects on the diffusion of receptors from actin corrals and lipid domains. Single-molecule tracking data acquired on living HeLa cells agree with the simulation results and the dynamic regulation mechanism that controls the diffusion of single-molecule receptors is clarified.

II. MODEL DESCRIPTION

Single-molecule tracking can effectively probe into the microscopic environment and thermal fluctuations of a receptor protein in a living cell. Although the plasma membranes of live cells are complex and highly heterogeneous,[7,19–21] the influences of cellular objects or structures far separated from a receptor protein are negligible for the description of single-molecule diffusion of the protein. Thus, to depict the diffusive behavior of a receptor protein we can focus on the local

a)Electronic mail: jyhuang@faculty.nctu.edu.tw

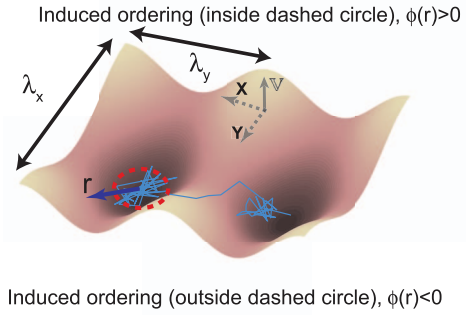

FIG. 1. Schematic showing the model that involves the structure of actin skeleton-induced membrane compartments, lipid raft domains, and dynamic protein complexes. The confinement effect by actin corral is modeled with a potential ($\mathbb{V}$) and the length scales (λ_x and λ_y). The region with induced lipid ordering (inside the red dashed circle) has $\phi(r) > 0$ for enriched raft lipids and outside has $\phi(r) < 0$ for depleted raft lipids.

environment of the protein. Based on our current knowledge of single-molecule diffusion in the plasma membrane, two types of interactions between a receptor protein and its local environment shall be taken into account. First, the receptor protein can induce a local ordering of the surrounding lipid molecules via a lipid-protein interaction.[22–24] The receptor can also serve as a nucleation site to form a stable lipid nanodomain and results in a free energy decrease. Second, there exist actin skeleton-induced membrane compartments.[25,26] Our model incorporates a cooperative action with the hierarchical structure of actin skeleton-induced membrane compartments, protein-induced lipid domains, and dynamic protein diffusion. The basic ideas of the model are illustrated in Fig. 1 with the protein-induced lipid ordering schematically represented as an area inside the red dashed circle and the actin skeleton-induced membrane compartment with a potential well of length scales λ_x and λ_y.

The diffusion of a receptor protein in the plasma membrane was simulated with the generalized Langevin equation[16]

$$m\gamma\partial_t\vec{x_k} = -\nabla_k(\mathbb{V}+\mathbb{F}) + \vec{f_k} = -\mathbb{U} + \vec{f_k}, \quad (1)$$

where subindex k represents the kth molecule at the position $\vec{x_k}$. The frictional parameter γ is relevant to the diffusion coefficient D with $m\gamma = k_BT/D$. For an actin-anchored protein, the confinement effect of actin corrals can be modeled with a potential $\mathbb{V}$. $\mathbb{F}$ incorporates the interactions of lipid-lipid and lipid-protein. Thus, the total force acting on the diffusive protein is expressed as $-\mathbb{U}$. The fluctuation force $\vec{f_k}$ experienced by the protein behaves like a Gaussian white noise with zero mean and a correlation satisfying the fluctuation-dissipation theorem $\langle \vec{f_k}(t)\vec{f_k}(t+\tau)\rangle = 2m\gamma k_BT\delta(\tau)$.

For a mixture of raft and non-raft lipids, the lipid-dependent segregation can result in lipid nanodomains with an order parameter $\phi(r)$ to reflect the degree of enrichment of raft lipids ($\phi(r) > 0$ inside the red dashed circle in Fig. 1 and $\phi(r) < 0$ outside the red dashed circle). The dynamic evolution of the order parameter $\phi(r)$ is governed by the Cahn–Hilliard equation[17,18]

$$\partial_t\phi(r,t) = D\nabla^2[\partial_\phi\mathbb{F}], \quad (2)$$

where $\mathbb{F}$ is the Ginzburg-Landau functional of lipid-lipid and lipid-protein interaction energy densities, and can be expressed as[17,27]

$$\mathbb{F} = \int\left[\frac{1}{2}\alpha\phi(r,t)^2 + \frac{1}{4}\beta\phi(r,t)^4 + \frac{1}{2}\chi|\nabla\phi(r,t)|^2 - \phi(r,t)S_P(r)\right]dA. \quad (3)$$

The Cahn-Hilliard equation is a coarse-grained version of Brownian-like diffusion.[28] According to the Landau mean field theory[17] of a physical system with an inversion symmetry $\phi(r) = \phi(-r)$, the first two terms of Eq. (3) reflect the thermal stability of the system. The parameter α represents the binding energy of lipids (i.e., the energy of removing a lipid molecule from the lipid membrane), β denotes the interaction strength between lipid molecules, and the third term is the line tension at the boundary of two different lipid phases. Typical values of the parameters are $\alpha = \frac{1}{2}k_BT$, $\beta = \frac{1}{3}k_BT$, and $\chi/\mu m^2 = 4k_BT$ for the plasma membrane system of live cells. The presence of a protein can generate a force field that breaks the symmetry of lipid phases. The symmetry breaking yields a linear term with negative value in $\mathbb{F}$.[17] Therefore, the lipid ordering $\phi(r) > 0$ induced by a protein ($S_P(r) = 1$) decreases the free energy in a lipid domain.

To describe the diffusive behavior of a protein with Eq. (1), we assumed that the fluctuation force $\vec{f_k}$ follows the Wiener process with a probability density function of

$$P_{W_t} = \frac{1}{\sqrt{2\pi t}}e^{-\frac{\vec{x}^2}{2t}}. \quad (4)$$

Thus we can rewrite Eq. (1) as

$$d\vec{x_k} = -\frac{\mathbb{U}}{m\gamma}dt + \sqrt{2D}dW_t = -\frac{\mathbb{U}D}{k_BT}dt + \sqrt{2D}dW_t. \quad (5)$$

By invoking the stochastic chain rule[29] on Eq. (5), we can obtain an equation of the squared displacement,

$$d\vec{x_k}^2 = -2\frac{\mathbb{U}D}{k_BT}\vec{x_k}dt + 2Ddt + 2\sqrt{2D}\vec{x_k}dW_t. \quad (6)$$

Note that the Wiener process yields the first- and the second-power expected values, $E[dW_t] = 0$ and $E[(dW_t)^2] = \Delta t$. Thus, from Eq. (6), we derived the mean-square and the variance of squared displacement as

$$\begin{aligned}\overline{d\vec{x_k}^2} &= E^2[d\vec{x_k}^2] \\ &= E^2\left[-2\frac{\mathbb{U}D}{k_BT}\vec{x_k}dt + 2Ddt + 2\sqrt{2D}\vec{x_k}dW_t\right] \\ &= \left(-2E\left[\frac{\mathbb{U}D}{k_BT}\vec{x_k}\right]\Delta t + 2D\Delta t\right)^2 \end{aligned} \quad (7)$$

and

$$
\begin{aligned}
&Var\left[(d\overrightarrow{x_k})^2\right] \\
&= E\left[\left(d\overrightarrow{x_k}^2\right)^2\right] - E^2\left[d\overrightarrow{x_k}^2\right] \\
&= E\left[\left(-2\frac{\mathbb{U}D}{k_BT}\overrightarrow{x_k}dt + 2Ddt + 2\sqrt{2D}\overrightarrow{x_k}dW_t\right)^2\right] \\
&\quad - \left(-2E\left[\frac{\mathbb{U}D}{k_BT}\overrightarrow{x_k}\right]\Delta t + 2D\Delta t\right)^2 \\
&= 8D\overline{x_k}^2\Delta t + 4Var\left[\frac{\mathbb{U}D}{k_BT}\overrightarrow{x_k}\right](\Delta t)^2, \qquad (8)
\end{aligned}
$$

where *Var* and *E* denote the variance and expected value. We defined a normalized variance of squared displacement as $V(R^2) = \mathrm{Var}(R^2)/(\overline{R^2})^2$, which yields

$$
\begin{aligned}
V(R^2) &= \frac{8D\overline{x_k}^2\Delta t + 4Var\left[\frac{\mathbb{U}D}{k_BT}\overrightarrow{x_k}\right](\Delta t)^2}{\left(-2E\left[\frac{\mathbb{U}D}{k_BT}\overrightarrow{x_k}\right]\Delta t + 2D\Delta t\right)^2} \\
&= \frac{2\frac{\overline{x_k}^2}{D\Delta t} + Var\left[\frac{\mathbb{U}\overrightarrow{x_k}}{k_BT}\right]}{\left(1 - E\left[\frac{\mathbb{U}\overrightarrow{x_k}}{k_BT}\right]\right)^2}. \qquad (9)
\end{aligned}
$$

Here $\overline{R_k}^2(t) = \overline{d\vec{x}_k^2(t)}$ denotes the local mean-square displacement (MSD). $V(R^2)$ can measure the relative influence of a deterministic force $-\mathbb{U}$ to that of the stochastic force $\overrightarrow{f_k} = m\gamma\sqrt{2D}dW(t)$.

For simplicity, we used a cosine function with different exponent $\mathbb{V} = \mathbb{V}_0 cos^n[\pi(\frac{x_k}{\lambda_x} + \frac{y_k}{\lambda_y})]cos^n[\pi(\frac{x_k}{\lambda_x} - \frac{y_k}{\lambda_y})]$ to model the action of actin corral on the receptor protein. Considering the extreme case with $n \gg 1$, the interaction range of the confinement potential can be estimated with $w = 2\frac{\lambda_x}{\pi}|cos^{-1}[(1/2)^{1/2n}]|$, then the deterministic force $-\nabla\mathbb{V}$ becomes $\mathbb{V}_0\frac{\pi}{\lambda_x}[\delta((x + w/2)\frac{\pi}{\lambda_x}) - \delta((x + \lambda_x - w/2)\frac{\pi}{\lambda_x})]$. Thus the normalized variance can be simplified as

$$
V(R^2) = \begin{cases} 2 & \text{Brownian motion} \\ \frac{2}{\left(1-\frac{\mathbb{V}_0\pi}{k_BT}\right)^2} & n \gg 1 \end{cases}. \qquad (10)
$$

For molecules under free diffusion (i.e., $\mathbb{U} = 0$), $V(R^2)$ has a constant value of 2, as shown by the red solid line in Fig. 2. As molecules diffuse under a confinement of actin corral, $V(R^2)$ increases from 2 with the confinement strength (see the blue solid curve of Fig. 2). When the deterministic force is much larger than the fluctuation force, $V(R^2)$ decreases monotonically as the deterministic force increases. A critical region lies in the between where $V(R^2)$ can be much larger than 2. Thus, the plot of $V(R^2)$ versus $\overline{R^2(t)}$ carries important information about local environment changes of receptor proteins in live cells.

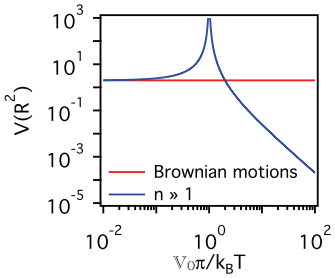

FIG. 2. The analytical expression of $V(R^2)$ for $n \gg 1$ is plotted as a function of the ratio of deterministic force and stochastic force.

III. METHODS

A. Cell culture and reagents

HeLa cells were cultured in Dulbecco's Modified Eagle's medium (DMEM) with 10%(*v*/*v*) fetal bovine serum without phenol red. Before single-molecule live-cell imaging, the cells were plated in a slide with eight-well chambers. After reaching 70%–80% confluence, the cells were deprived of serum for 24 h. To label EGFR, the cells were incubated with 10 nM of anti-EGFR antibody (Thermo Scientific) for 15 min and washed three times with phosphate buffered saline (PBS). The cells were then treated with IgG-Qdot-525 for 15 min and washed three times again with PBS. To synthesize fluorescent EGF, Biotin-EGF (from Invitrogen) was conjugated to Qdot-585-streptavidin in PBS. The resulting product was denoted as Qdot-585-EGF. The cells can be stimulated with the Qdot-585-EGF at a concentration of 40 ng/ml. The concentration of Qdot-585-EGF was increased to 0.4 μg/ml to provoke actin polymerization.

B. Single-molecule optical measurement

Single-molecule fluorescence was measured with an inverted optical microscope (Olympus IX-71) equipped with a high numerical aperture (NA) oil immersion objective lens (APON 60XOTIRFM, NA 1.45, Olympus). The output from a blue (473 nm) solid-state laser was collimated and sent to the back focal plane of the objective lens to excite the quantum dots in live cells. The same objective lens was used to collect the fluorescent signal from the sample. The fluorescent signals were filtered with a 473 nm Raman notch filter and then detected with an electron-multiplying charge coupled device (EMCCD, Cascade II 512 from Photometrics). The measurement procedure was controlled by a software based on μ-manager.

C. Data analysis

Coordinates of two-dimensional positions of single-molecule receptors were extracted from a set of fluorescent images. The nearest positions in consecutive frames were connected to form single-molecule trajectories using multiple-target tracing algorithm.[30] We extracted the events of confined diffusion from a single-molecule trajectory by using the confinement quantification procedure,[31] which had been demonstrated to be highly reliable to distinguish the events of confined diffusion from hopping. After retrieving the events of confined diffusion from we calculated the local squared displacements with every three consecutive frames. A

histogram of local squared displacements $\overline{R^2}$ and normalized variances $V(R^2)$ was presented in a 2D contour plot.

D. Simulation

We discretized the generalized Langevin equation (Eq. (1)) and solved the discrete form with Euler scheme. To simulate lipid dynamics with the Cahn–Hilliard equation (Eq. (2)), we assumed that lipid diffusion is ten times faster than receptor protein. Thus, time mesh of lipid diffusion Δt_l was chosen to be 0.25 ms with the same spatial mesh $\Delta x_l = \Delta x_p = 50$ nm. To synchronize the dynamical evolutions of the protein and lipid molecules, the lipid environment was adjusted to every change of protein's position and the lipid-protein interaction ($\mathbb{F}$ in Eq. (2)) was updated accordingly. The initial structure of lipid environment was assumed to be a homogeneous mixture with $x1\%$ of raft lipids and $x2\%$ of non-raft lipids, giving $\phi_0 = (x1 - x2)/100$. The parameter α, β, and $\chi/\mu\text{m}^2$ in our simulation were chosen to be $\frac{1}{2}k_BT$, $\frac{1}{3}k_BT$, and $4k_BT$. In addition to the lipid-lipid and lipid-protein interactions described by $\mathbb{F}$, the driving force in the generalized Langevin equation involves an anchoring potential $\mathbb{V}$ from actin corral. We conducted the simulation with $\mathbb{V}_0 = 0.05$ eV and $\lambda_x = \lambda_y = 70$ nm.[25] To properly compare the simulated results with experimental data, the squared displacement and normalized variance were binned with various time durations from 2.5 to 25 ms.

IV. RESULTS

A. Confinement effect of receptor protein by actin corral

To elaborate the confinement of a receptor protein by actin corrals, we simulated the trajectories of the protein with different $\mathbb{V}_0$, profile index n, and length scales λ_x and λ_y. The simulation was performed by positioning a receptor protein at the center of actin corral and Eqs. (1) and (2) were solved self consistently. From the single-molecule trajectories, we calculated the local MSD $R^2_\tau(t) = \{[\vec{x}(t+\tau) - \vec{x}(t)]^2 + [(\vec{x}(t) - \vec{x}(t-\tau)]^2\}/2$ with a sampling period τ and the normalized variance $V(R^2)$ as a function of diffusion coefficient. The results are presented in Figs. 3 and 4.

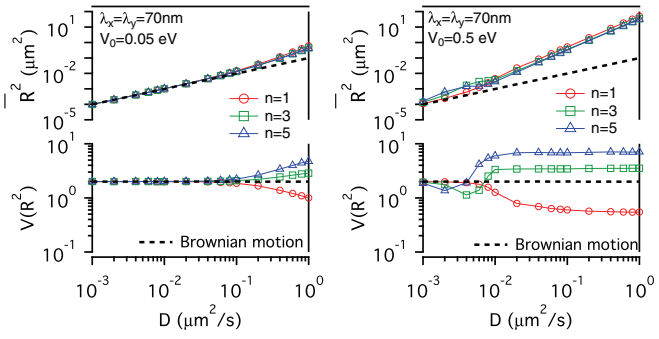

FIG. 3. $\overline{R^2}$-D and $V(R^2)$-D of single-molecule receptors under (a) weak ($\mathbb{V}_0 = 0.05$ eV, $\lambda_x = \lambda_y = 70$ nm) and (b) medium confinement strength ($\mathbb{V}_0 = 0.5$ eV, $\lambda_x = \lambda_y = 70$ nm) with different confinement profiles ($n = 1, 3, 5$) of actin corrals.

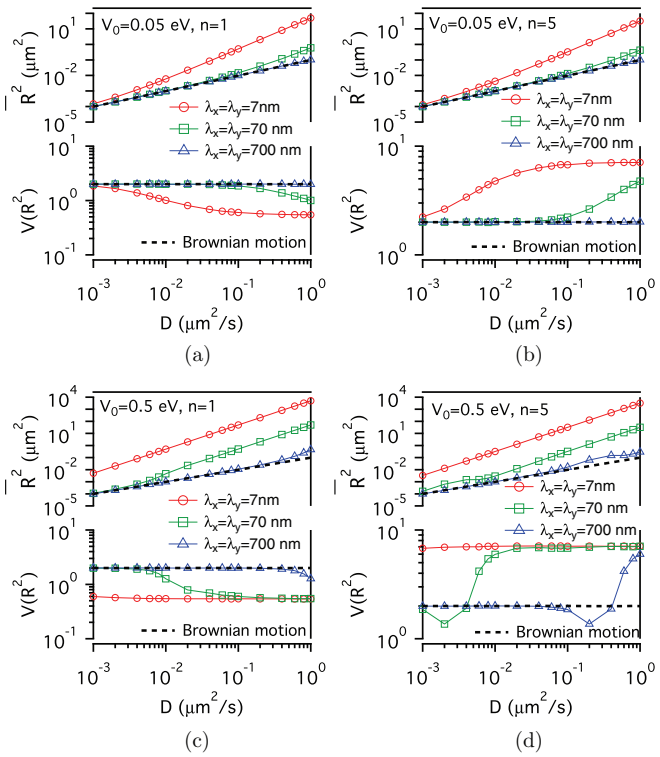

FIG. 4. $\overline{R^2}$-D and $V(R^2)$-D of single-molecule receptors with (a) and (b) low ($\mathbb{V}_0 = 0.05$ eV) and (c) and (d) high confinement amplitude ($\mathbb{V}_0 = 0.5$ eV) with different potential profiles ($n = 1, 5$) and actin corral sizes (red open circles: $\lambda_x = \lambda_y = 7$ nm, green open squares: 70 nm, and blue open triangles: 700 nm).

Fig. 3 depicts how the confinement strength and profile of actin corral affect the diffusive behaviors of receptor proteins. At weak confinement strength, $\overline{R^2}$-D follows closely the line of Brownian diffusion, which has a slope of 4τ. Only those fast species with $\overline{R^2(t)}$ larger than the length scales of confinement can experience the potential. That causes $\overline{R^2(t)}$ to deviate from the line of free diffusion. The resulting slope increases with $\mathbb{V}_0$, yielding an effective diffusion coefficient of $D_{eff} = \overline{R^2}/D$. The slope of $\overline{R^2}$-D does not change with n. However, at sufficiently fast diffusion $V(R^2)$ levels off to different values that sensitively depend on n. This saturation behavior can be understood as follows: For $n = 3, 5$, the proportionality of Var(R^2)-D is larger than that of $\overline{R^2}$-D, causing the normalized $V(R^2) = \text{Var}(R^2)/(\overline{R^2})^2$ to saturate at a higher value as D increases. For $n = 1$, the proportionality of Var(R^2)-D is smaller than that of $\overline{R^2}$-D, which results in $V(R^2)$ to saturate at a level lower than 2 (see Fig. 3(b)). By summarizing the simulation results, the level-off values of $V(R^2)$ depend sensitively on the confinement profile and the D value where $V(R^2)$ starts to deviate from 2 depends on $\mathbb{V}_0$.

Fig. 4 is similar to Fig. 3 but with different sizes of actin corral. From the simulation, a strong confinement condition of actin corral can be achieved with $\mathbb{V}_0 = 0.5$ eV and $\lambda_x = \lambda_y = 7$ nm; whereas a weak confinement condition can be produced with $\mathbb{V}_0 = 0.05$ eV and $\lambda_x = \lambda_y = 700$ nm.

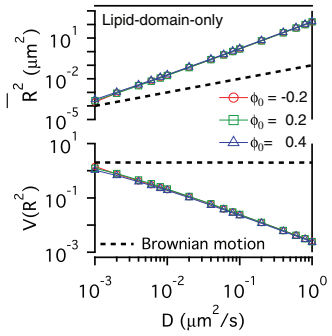

FIG. 5. The confinement effect of lipid raft domain on $\overline{R^2}$-D and $V(R^2)$-D of single-molecule receptors. In the simulation, three different homogeneous mixtures of lipids with $\phi_0 = -0.2$ (red open circles), 0.2 (green open squares), and 0.4 (blue open triangles) were prepared.

B. Influence of lipid raft domains on the diffusion of receptor protein

When a receptor protein moves in a lipid environment, it can restructure the local environment via a protein-lipid interaction. To simulate the restructuring dynamics, we prepared an initial homogeneous lipid mixture with 40% raft lipids and 60% non-raft lipids ($\phi_0 = -0.2$), 60% raft lipids and 40% non-raft lipids ($\phi_0 = 0.2$), and 70% raft lipids and 30% non-raft lipids ($\phi_0 = 0.4$), respectively.

Fig. 5 shows that the protein-induced lipid ordering domain increases $\overline{R^2}$ of receptor in the entire range of D used in the simulation, and yields higher $\overline{R^2}$-D slope than that of free diffusion (dashed line). The increased slope does not depend on ϕ_0. In contrast, $V(R^2)$ of receptor in a lipid raft domain decreases monotonically as D increases. Owing to the protein-lipid interaction, the receptor protein can induce an increased ordering $\phi(r)$ on nearby raft lipids. The protein and the surrounding ordered lipids can be viewed as a dressed protein. The faster the protein diffuses, the larger the dressing effect is. This leads to Var(R^2) a weaker function of D than that of $\overline{R^2}$, rendering $V(R^2)$ to decrease monotonically with increasing D.

C. Influences of both actin corrals and lipid raft domains on the diffusion of receptor protein

We can distinguish a subtle difference in the confinement effects from actin corrals and lipid raft domains. The difference can be understood by noting that the influence of lipid raft domain on a receptor protein originates from an induced ordering of raft lipids, which yields a dressing effect on the receptor protein. In contrast, the interaction between actin filaments and the confined protein is simulated with a potential. The force experienced by the protein depends on the protein's position, which is stochastic due to thermal fluctuation. Thus, it is interesting to investigate further how $\overline{R^2(t)}$ and $V(R^2)$ of single-molecule trajectories are affected by the combined effects from actin corrals and lipid raft domains.

Fig. 6 exhibits the influences from lipid domains and actin corrals with two different potential profiles ($n = 1$ and $n = 5$). Under the weak confinement condition of actin corrals shown in Figs. 6(a) and 6(d), the variations of $\overline{R^2(t)}$ and $V(R^2)$ are dominated by lipid domains. The curves of $V(R^2)$-D start to level off at $D = 0.2\ \mu m^2/s$. Figs. 6(b) and 6(e) present the results with medium actin confinement strength. For $n = 1$ (see Fig. 6(b)), the confined force is nonnegligible at the center of actin corral. $V(R^2)$ remains close to 2 in the range of $0.001\ \mu m^2/s < D < 0.006\ \mu m^2/s$, indicating that the influence from lipid domains is compensated by that from actin corrals. As $D > 0.006\ \mu m^2/s$, $V(R^2)$ decreases from 2 and then saturates to a value, depending on the strength of actin confinement. For $n = 5$, the confined force is negligible at the center of actin corral. The variation of $V(R^2)$ is dominated by the lipid raft domains; $V(R^2)$ decreases from 2 as $D > 0.001\ \mu m^2/s$. It then levels off at $D = 0.04\ \mu m^2/s$ owing to the action of actin corrals. For the case with strong actin confinement shown in Figs. 6(c) and 6(f), the $\overline{R^2(t)}$-D

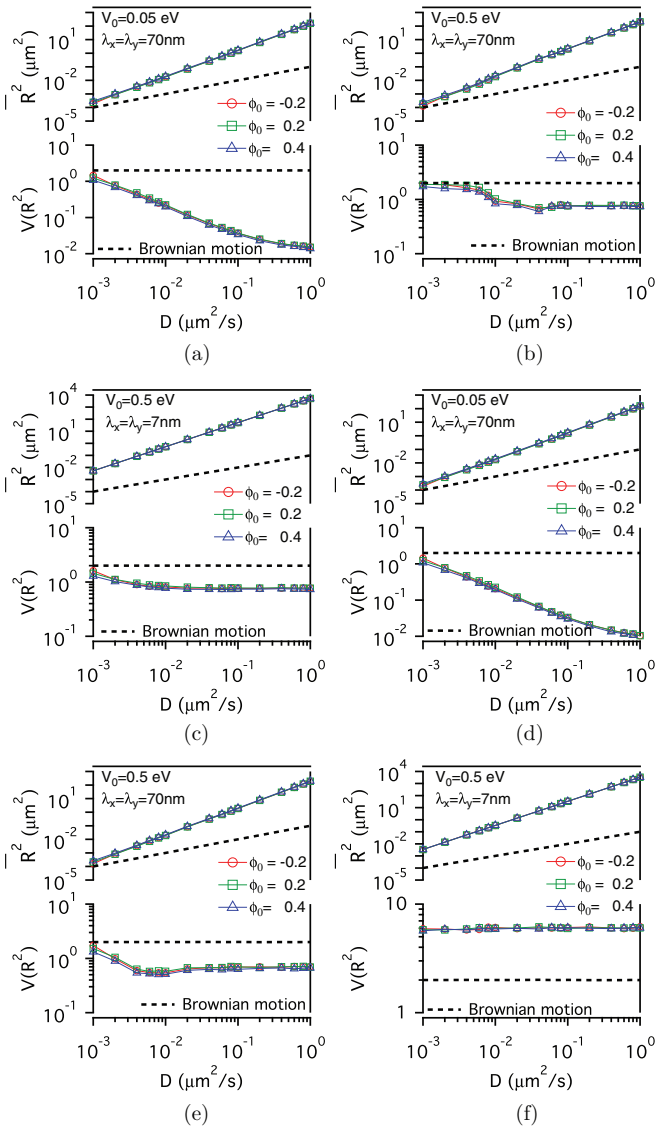

FIG. 6. The results of simulation on the confinement influences from both lipid domains (with different initial lipid compositions: $\phi_0 = -0.2, 0.2, 0.4$) and actin corrals: (a) weak ($\mathbb{V}_0 = 0.05$ eV, $\lambda_x = \lambda_y = 70$ nm); (b) medium ($\mathbb{V}_0 = 0.5$ eV, $\lambda_x = \lambda_y = 70$ nm); and (c) strong ($\mathbb{V}_0 = 0.5$ eV, $\lambda_x = \lambda_y = 7$ nm) confinement strength. The potential profile index is $n = 1$ in (a), (b), (c); $n = 5$ in (d), (e), (f).

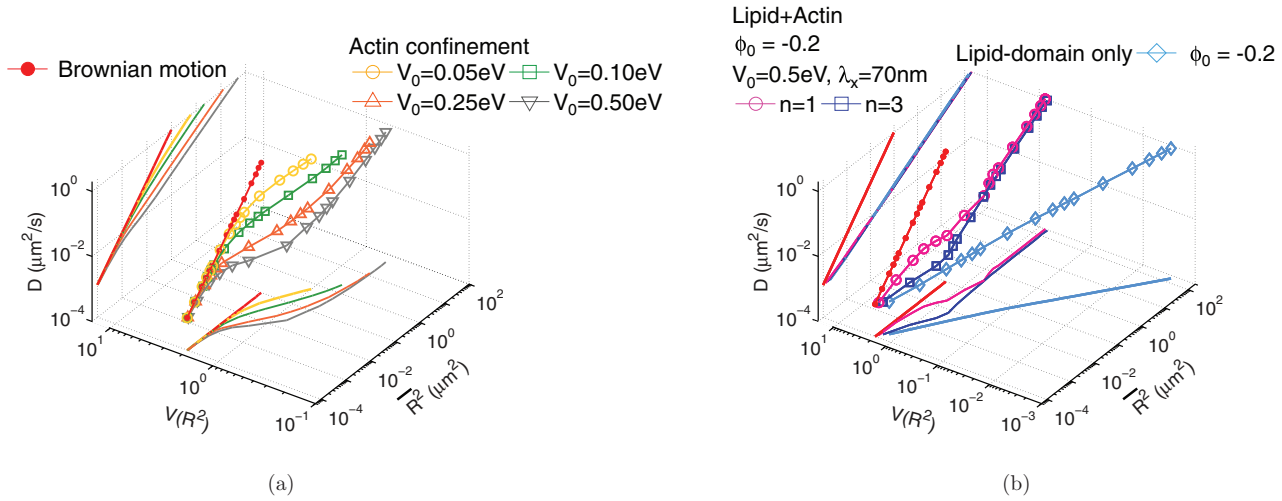

FIG. 7. (a) Simulated confinement effects from actin corrals alone with different confinement potentials ($\mathbb{V}_0 = 0.05$, 0.1, 0.25, and 0.5 eV; $\lambda_x = \lambda_y = 70$ nm; $n = 1$) are plotted in the $V(R^2)$-$\overline{R^2}$-D space. In the simulation, the diffusion coefficient (D) was varied from $D = 10^{-3}\,\mu\text{m}^2/\text{s}$ to $D = 10^{0}\,\mu\text{m}^2/\text{s}$. (b) $V(R^2)$-$\overline{R^2}$-D plots showing confinement effects from both actin corrals ($\mathbb{V}_0 = 0.5$ eV; $\lambda_x = \lambda_y = 70$ nm; $n = 1$, 3) and lipid domains ($\phi_0 = -0.2$) or from lipid domains alone.

curves shift upward with the same slope as the previous cases. In Fig. 6(c) with $n = 1$, $V(R^2)$ decreases from 2 as $D > 0.001\,\mu\text{m}^2/\text{s}$ and then levels off at $D > 0.01\,\mu\text{m}^2/\text{s}$. For $n = 5$ (Fig. 6(f)), the confinement force is strong in the entire D range; $V(R^2)$ is kept at a constant level that reflects the confinement strength of actin.

To better elaborate the diffusion behaviors of receptor proteins in a heterogeneous lipid environment, the simulation results are presented in a 3D plot of D-$V(R^2)$-$\overline{R^2(t)}$. In Fig. 7(a), the influences on a receptor protein from actin corrals alone with different confinement potentials ($\mathbb{V}_0 = 0.05$, 0.1, 0.25, and 0.5 eV; $\lambda_x = \lambda_y = 70$ nm; $n = 1$) are shown with open symbols. For comparison, the diffusive behavior of Brownian motion is described with red solid circles. The slope of D-$\overline{R^2(t)}$ decreases as $\mathbb{V}_0$ increases; whereas the $V(R^2)$-$\overline{R^2(t)}$ curves first decrease and then saturate at the same level; the $\overline{R^2(t)}$ value where $V(R^2)$ starts to deviate from 2 depends on $\mathbb{V}_0$. The confinement effects from both actin corrals and lipid domains or from lipid domains alone are presented in Fig. 7(b). Lipid domain decreases $V(R^2)$ of receptor as $\overline{R^2(t)}$ is increased. However, as actin corrals appear, the smallest $V(R^2)$ is limited by the confinement effect of actin corrals. The different potential profiles ($n = 1$,3) can result in different $V(R^2)$-$\overline{R^2(t)}$ curves, but these curves are projected to the same line on the D-$\overline{R^2(t)}$ plane.

D. Experimental verification of the confinement effects of actin corrals and lipid raft domains on the diffusion of epidermal growth factor receptors (EGFRs) in live HeLa cells

We provided experimental evidences of the confinement effects of actin corrals and lipid domains on the diffusion of EGFR with single-molecule tracking technique. The EGFR proteins of live HeLa cells were labeled with Qdot-525 quantum dots conjugated EGFR antibody (Qdot525-Ab-EGFR). We activated the cells with fluorescent EGF (Qdot585-EGF). The measured single-molecule trajectories of unliganded (Ab-Qdot525)-EGFR and liganded (EGF-Qdot585)EGFR on live HeLa cells are presented in Fig. 8. Both of the EGFR species exhibit confined diffusion (see region 1 marked with the red spots) interspaced by hopping motions occurring in region 2. To separate the events of confined diffusion in single-molecule trajectories from hopping motions, we employed the confinement quantification procedure developed by Meilhac *et al.*[31]

After retrieving the events of confined diffusion from single-molecule trajectories, we calculated the local squared displacements $\overline{R^2}$ and the normalized variance of the squared displacements $V(R^2)$. The localization accuracy of our single-molecule optical apparatus was about 40 nm, implying an

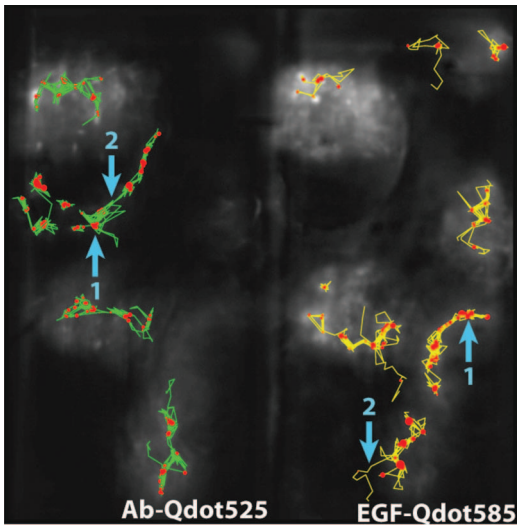

FIG. 8. Single-molecule trajectories of unliganded (Ab-Qdot525)-EGFR (green) and liganded (EGF-Qdot585)EGFR (yellow) superimposed on a dark field image of the live HeLa cells. The regions of confined diffusion are marked with the red spots.

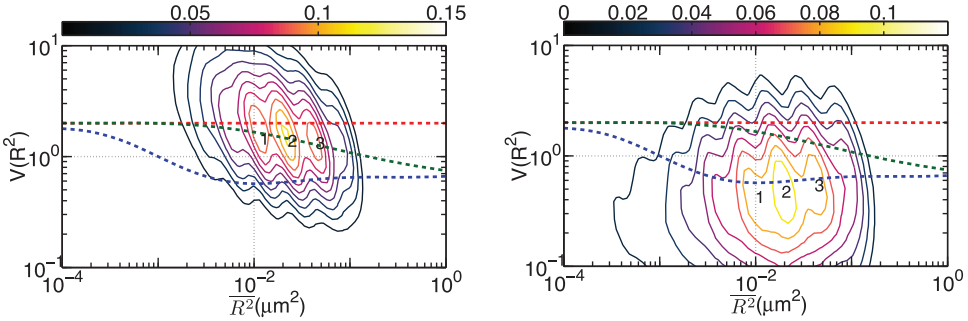

FIG. 9. (a) The plot of $V(R^2) - \overline{R^2}$ for unliganded Qdot525-Ab-EGFR on living HeLa cells at rest. Simulated curves of the peak positions for receptor molecules under free Brownian motion (the red dashed line), diffusion under the confinement of actin corrals alone (the green dashed line), or both the actin corrals and lipid raft domains (the blue dashed line) are included for comparison. (b) The same plot for liganded Qdot585-EGF-EGFR in activated cells by Qdot585-EGF.

accuracy of 0.002 μm^2 for $\overline{R^2(t)}$ determination. A histogram of $\overline{R^2}$ versus $V(R^2)$ was presented in a 2D contour plot (see Figs. 9 and 10). An attractive feature of the data visualization scheme is that when a molecule repetitively visits (or stays long enough in) a membrane domain, the characteristic $\overline{R^2}$ and $V(R^2)$ of the domain will be imposed on the trajectory, and therefore yields a peak feature at the corresponding position on the plot.

Fig. 9(a) presents the data from unliganded EGFRs at rest taken one frame per $\tau = 25$ ms. Among the three peaks, labeled 1, 2, and 3 in Fig. 9(a), the peak 2 was the highest stable and most populated state given that the forward rate constant was $k_f(2 \rightarrow 3) = 3.7$ s^{-1}, which was lower than that of the other forward kinetic process $k_f(1 \rightarrow 3) = 10.2$ s^{-1} and the backward rate constants $k_b(3 \rightarrow 1) = 32.4$ s^{-1} and $k_b(3 \rightarrow 2) = 39.3$ s^{-1}. The three peaks were located at the ($\overline{R^2}$, $V(R^2)$) coordinates of (0.01, 1.45), (0.02, 1.39), and (0.04, 1.33), respectively. The simulated curves presented in Fig. 7 for receptor molecules under free Brownian motion (red dashed line), under the confinement by actin corrals alone (green dashed curve), or by both the actin corrals and lipid domains (blue dashed curve), were included for comparison. The peak positions of the three states fell on the curve of the actin confinement, indicating that these unliganded receptor molecules were not free diffusers, but instead confined by actin corrals alone.

With the EGFR at rest as the control, we further examined the diffusion kinetics of liganded Qdot585-EGF-EGFR. Figure 9(b) shows the $V(R^2) - \overline{R^2}$ plot of the liganded EGFR on activated cells by Qdot585-EGF. Three peaks were found to locate at (0.01, 0.42), (0.02, 0.47), and (0.04, 0.54) with associated forward transition rate constants of $k_f(1 \rightarrow 3) = 4.8$ s^{-1} and $k_f(2 \rightarrow 3) = 5.1$ s^{-1}. These three peak positions agreed better with the model that includes the confinement effects of both actin corrals and lipid domains. Pretreating the cells with nystatin and then activated with Qdot585-EGF (data not shown here) reduced the forward rate constants to $k_f(1 \rightarrow 3) = 3.4$ s^{-1} and $k_f(2 \rightarrow 3) = 3.6$ s^{-1}, which were similar to those of the unliganded EGFR at rest. Perhaps because unliganded EGFRs at rest are located outside the lipid domains, EGF binding caused the receptors to move into the lipid domains. Pretreatment of cells with nystatin sequestered the membrane cholesterol and disrupted the lipid domains. This leads to local environmental changes in the ligand bound EGFR and reduced the rate constants of the diffusion kinetics.

The simulation results presented in Fig. 4 suggest that the confinement strength of actin corral can be increased by

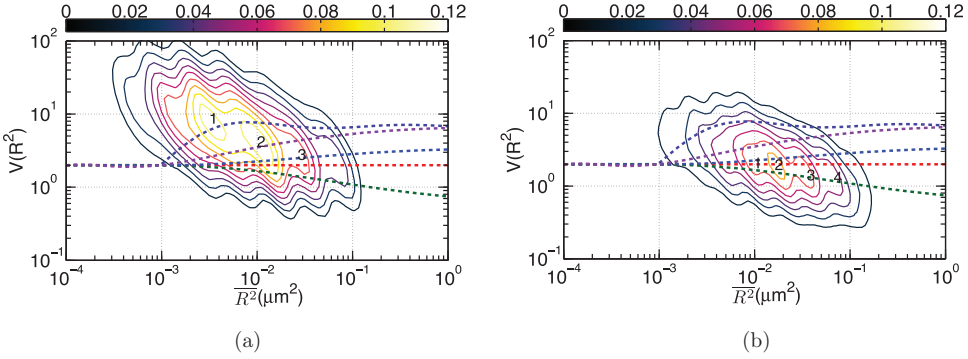

FIG. 10. (a) The plot of $V(R^2) - \overline{R^2}$ of Qdot585-EGF-EGFR trajectories in highly stimulated HeLa cells. (b) The plot of $V(R^2) - \overline{R^2}$ of Qdot585-EGF-EGFR trajectories on the Cytochalasin D treated cells. The red dashed curve is the simulation result of Brownian motion; the green dashed line is the simulation result with the confinement of actin corrals using $L_x = L_y = 70$ nm, $\mathbb{V}_0 = 0.1$ eV, $n = 1$; the blue dashed line is the result with $L_x = L_y = 70$ nm, $\mathbb{V}_0 = 0.1$ eV, $n = 3$; the purple dashed line: $L_x = L_y = 70$ nm, $\mathbb{V}_0 = 0.15$ eV, $n = 5$; and the indigo dashed line: $L_x = L_y = 70$ nm, $\mathbb{V}_0 = 0.5$ eV, $n = 5$.

either increasing $\mathbb{V}_0$ or reducing the actin corral size. Lipid raft domains contain several kinds of actin-anchored proteins including EGFR. Thus, it is possible to reduce the actin corral size by promoting the actin polymerization.[32,33] This can be done by using a high dosage of EGF to stimulate the HeLa cells. The stronger actin corral confinement shall increase $V(R^2)$ of EGFR. The experimental result is presented in Fig. 10(a), revealing clearly that $V(R^2)$ of EGFRs in the highly stimulated cells is increased to as high as 8. The three peaks shown exhibit different $V(R^2)$, suggesting that the EGFRs are confined by actin corrals with different strengths. The actin filaments in the cells can be depolymerized by treating the cells with Cytochalasin D. The result shown in Fig. 10(b) exhibits smaller $V(R^2) - \overline{R^2}$, indicating weaker confinement strengths of actin corrals.

V. DISCUSSIONS

Information theory provides an insightful perspective on the optimal strategy that live cells can take to organize their signaling receptor proteins. However, real situation in living eukaryotic cells is much more complex. It is important to built an energetic model that involves a hierarchical structure of actin skeleton-induced membrane compartments, lipid domains, and dynamic protein complexes to verify the underlying processes to be energetically favorable. A detailed microscopic understanding of a single-molecule system is often precluded by a complex environment and thermal fluctuations. In this paper, we developed a formalization that captures the sensitivity of single-molecule processes, statistic accuracy of data analysis, and the hierarchical structure of plasma membranes. Based on the model, we also proposed a convenient data visualization scheme to help extracting important information from single-molecule trajectories.

The normalized variance measures the relative influence of a deterministic force to that of the stochastic fluctuating force. Only diffusion species with $\overline{R^2(t)}$ larger than the confined area can experience the force of actin corrals. That causes $V(R^2)$ levels off to different values, which depend on the potential profile. In contrast, for a receptor protein confined in a lipid domain, the protein can induce an ordering of its surrounding lipid molecules and is dressed. The faster the protein diffuses, the larger dressing effect it has. This results in $V(R^2)$ monotonically decreasing as D increases. The confinement effects from actin corrals and lipid domains have opposite influence on $V(R^2)$.

We applied single-molecule tracking technique to probe the diffusive behaviors of unliganded and liganded EGFR on living HeLa cells. Our data visualization scheme suggests that EGFRs at rest probably are located outside the lipid raft domains. EGF binding causes the receptors to move into the lipid domains. Using a high dosage of EGF to provoke actin polymerization results in stronger actin corral confinement that raises $V(R^2)$ of the activated EGFRs above the limit of $V(R^2) = 2$.

Some membrane proteins are enriched in lipid raft domains for trafficking, endocytosis, and some specialized functions of biochemical reactions.[34–38] Recent computational study of protein-raft interaction also showed that lipid raft domain can enhance inter-protein collisions[22] and serves as a reactive center that can augment protein–protein interaction at nanometer scales.

VI. CONCLUSIONS

In summary, we developed an energetic model that captures the sensitivity of single-molecule processes, statistic accuracy of data analysis, and the hierarchical structure of plasma membranes of live cells. Simulation results on the diffusive trajectories of receptor proteins under varying confinements from actin corrals and lipid raft domains were presented with a plot of normalized variance $V(R^2)$ versus $\overline{R^2(t)}$. An attractive feature of this data visualization scheme is that when a molecule repetitively visits a membrane domain, the characteristic $\overline{R^2}$ and $V(R^2)$ of the domain will be imposed on the trajectory; this yields a peak feature at the corresponding position on the plot. Single-molecule tracking data acquired on living HeLa cells agree with the simulation results and the underlying mechanism that controls the diffusion of single-molecule receptors is therefore clarified. We also discovered that after ligand binding, EGFR molecules may move into lipid raft domains, whereas unliganded species remain outside the lipid domains. Our energetic model can provide a useful platform for further development to improve our understanding of how the mobile active clustering process of receptors and membrane structure regulates signal transduction.

ACKNOWLEDGMENTS

The authors thank the National Science Council of the Republic of China for its financial support under Grant No. NSC100-2112-M-009-015-MY3.

[1] R. Sharan, S. Suthram, R. M. Kelley, T. Kuhn, S. McCuine, P. Uetz, T. Sittler, R. M. Karp, and T. Ideker, Proc. Natl. Acad. Sci. U.S.A. **102**, 1974 (2005).
[2] J. M. Vaquerizas, S. K. Kummerfeld, S. A. Teichmann, and N. M. Luscombe, Nat. Rev. Genet. **10**, 252 (2009).
[3] N. Yosef, L. Ungar, E. Zalckvar, A. Kimchi, M. Kupiec, E. Ruppin, and R. Sharan, Mol. Syst. Biol. **5**, 248 (2009).
[4] L. Hodgkinson and R. M. Karp, Proc. Natl. Acad. Sci. U.S.A. **110**, 10872 (2013).
[5] J. E. Purvis and G. Lahav, Cell **152**, 945 (2013).
[6] G. Iyengar and M. Rao, Proc. Natl. Acad. Sci. U.S.A. **111**, 12402 (2014).
[7] D. Lingwood and K. Simons, Science **327**, 46 (2010).
[8] D. M. Owen, A. Magenau, D. Williamson, and K. Gaus, BioEssays **34**, 739 (2012).
[9] G. D. Paolo and P. D. Camilli, Nature (London) **443**, 651 (2006).
[10] J. Saarikangas, H. Zhao, and P. Lappalainen, Physiol. Rev. **90**, 259 (2010).
[11] T. Balla, Physiol. Rev. **93**, 1019 (2013).
[12] M. P. Sheetz, J. E. Sable, and H.-G. Döbereiner, Annu. Rev. Biophys. Biomol. Struct. **35**, 417 (2006).
[13] K. Jaqaman and S. Grinstein, Trends Cell Biol. **22**, 515 (2012).
[14] N. C. Gauthier, T. A. Masters, and M. P. Sheetz, Trends Cell Biol. **22**, 527 (2012).
[15] A. Kusumi, T. K. Fujiwara, N. Morone, K. J. Yoshida, R. Chadda, M. Xie, R. S. Kasai, and K. G. Suzuki, Seminars Cell Develop. Biol. **23**, 126 (2012).
[16] R. Zwanzig, *Nonequilibrium Statistical Mechanics* (Oxford University Press, 2001).
[17] A. Bray, Adv. Phys. **43**, 357 (1994).
[18] J. W. Cahn and J. E. Hilliard, J. Chem. Phys. **28**, 258 (1958).

[19]H. A. Lucero and P. W. Robbins, Arch. Biochem. Biophys. **426**, 208 (2004).
[20]A. Viola and N. Gupta, Nat. Rev. Immunol. **7**, 889 (2007).
[21]K. Simons and J. L. Sampaio, Cold Spring Harb. Perspect. Biol. **3**, a004697 (2011).
[22]D. V. Nicolau, Jr., K. Burrage, R. G. Parton, and J. F. Hancock, Mol. Cell. Biol. **26**, 313 (2006).
[23]S. Türkcan, M. U. Richly, A. Alexandrou, and J.-B. Masson, PLoS ONE **8**, e53073 (2013).
[24]D. L. Parton, A. Tek, M. Baaden, and M. S. P. Sansom, PLoS Comput. Biol. **9**, e1003034 (2013).
[25]K. Murase, T. Fujiwara, Y. Umemura, K. Suzuki, R. Iino, H. Yamashita, M. Saito, H. Murakoshi, K. Ritchie, and A. Kusumi, Biophys. J. **86**, 4075 (2004).
[26]A. Kusumi, C. Nakada, K. Ritchie, K. Murase, K. Suzuki, H. Murakoshi, R. S. Kasai, J. Kondo, and T. Fujiwara, Annu. Rev. Biophys. Biomol. Struct. **34**, 351 (2005).
[27]J. Gómez-Llobregat, J. Buceta, and R. Reigada, Sci. Rep. **3**, 2608 (2013).
[28]T. Speck, J. Bialké, A. M. Menzel, and H. Löwen, Phys. Rev. Lett. **112**, 218304 (2014).
[29]B. Øksendal, *Stochastic Differential Equations: An Introduction with Applications* (Springer, 2010).
[30]A. Sergé, N. Bertaux, H. Rigneault, and D. Marguet, Nat. Methods **5**, 687 (2008).
[31]N. Meilhac, L. L. Guyader, L. Salomé, and N. Destainville, Phys. Rev. E **73**, 011915 (2006).
[32]P. Rijken, W. Hage, P. van Bergen en Henegouwen, A. Verkleij, and J. Boonstra, J. Cell Sci. **100**, 491 (1991).
[33]M. P. Peppelenbosch, L. G. Tertoolen, W. J. Hage, and S. W. de Laat, Cell **74**, 565 (1993).
[34]C. Dietrich, Z. N. Volovyk, M. Levi, N. L. Thompson, and K. Jacobson, Proc. Natl. Acad. Sci. U.S.A. **98**, 10642 (2001).
[35]N. Kahya, D. A. Brown, and P. Schwille, Biochemistry **44**, 7479 (2005).
[36]S. J. Plowman, C. Muncke, R. G. Parton, and J. F. Hancock, Proc. Natl. Acad. Sci. U.S.A. **102**, 15500 (2005).
[37]M. Kirkham, A. Fujita, R. Chadda, S. J. Nixon, T. V. Kurzchalia, D. K. Sharma, R. E. Pagano, J. F. Hancock, S. Mayor, and R. G. Parton, J. Cell. Biol. **168**, 465 (2005).
[38]B. Rotblat, I. A. Prior, C. Muncke, R. G. Parton, Y. Kloog, Y. I. Henis, and J. F. Hancock, Mol. Cell. Biol. **24**, 6799 (2004).